NASA Technical Memorandum 102805

Wake Coupling to Full Potential Rotor Analysis Code

Francisco J. Torres, I-Chung Chang, and Byung K. Oh

August 1990

National Aeronautics and
Space Administration

NASA Technical Memorandum 102805

Wake Coupling to Full Potential Rotor Analysis Code

Francisco J. Torres and I-Chung Chang
Ames Research Center, Moffett Field, California

Byung K. Oh
Boeing Computer Services - Helicopters Support
Philadelphia, Pennsylvania

August 1990

National Aeronautics and
Space Administration

Ames Research Center
Moffett Field, California 94035-1000

NOMENCLATURE

B65	rotor analysis and performance code
TFAR1	quasi-steady potential code
TFAR2	full unsteady potential code
α_{B65}	total angle of attack of B65 code
α_{pitch}	angle of attack used as potential-code pitch-angle input
Θ	geometric angle of attack
Ψ	blade azimuth angle
r/R	blade span station
X/C	nondimensional chord length
Φ_{inflow}	inflow angle
Φ_{wake}	downwash contribution to inflow angle
ΔC_p	pressure coefficient (upper – lower)
μ	advance ratio
ΩR	blade tip speed
a_∞	far field speed of sound
V	flight velocity
VN_{near}	normal near-wake induced velocity
VN_{mid}	normal mid-wake induced velocity
VN_{far}	normal far-wake induced velocity
VT_{near}	tangential near-wake induced velocity
VT_{mid}	tangential mid-wake induced velocity
VT_{far}	tangential far-wake induced velocity
VN_{tot}	total normal induced velocity
VT_{tot}	total tangential induced velocity
$V_{1,2,3}$	velocity components due to blade motion
$q_{1,2,3}$	total velocity components
$\phi_{x,y,z}$	perturbation velocity components

WAKE COUPLING TO FULL POTENTIAL ROTOR ANALYSIS CODE

Francisco J. Torres, I-Chung Chang
NASA Ames Research Center, Moffett Field, California

Byung K. Oh
Boeing Computer Services - Helicopters Support, Philadelphia, Pennsylvania

SUMMARY

The wake information from a helicopter forward flight code is coupled with two transonic potential rotor codes. The induced velocities for the near-, mid-, and far-wake geometries are extracted from a nonlinear rigid wake of a standard performance and analysis code. These, together with the corresponding inflow angles, computation points, and azimuth angles, are then incorporated into the transonic potential codes. The coupled codes can then provide an improved prediction of rotor-b'ade loading at transonic speeds.

INTRODUCTION

It has been shown that the induced velocities encountered by a rotating blade significantly affect the inflow angle which in turn affects the total angle of attack which results in higher airloads (ref. 1). Most finite-difference or finite-volume rotor flow codes solve for the flow in the immediate vicinity of the blade and thereby neglect the effects of the wake, which can extend far from the computational domain. In this paper, the wake generated by a forward-flight performance and analysis code (B65) was extracted and implemented into a quasi-steady potential code (TFAR1) as well as a full unsteady potential code (TFAR2). The total induced velocity due to the wake was calculated by adding together the induced velocities from the near-, mid-, and far-wake regions. This total was then added to the flow velocity at the surface of the blade to incorporate the necessary wake effect in the calculations.

The B65 code has been made available through a memorandum of understanding with Boeing Helicopters. We would like to thank L. Dadone and W. E. Hooper of Boeing Helicopters for their support.

B65 CODE

The B65 code is a rotor aerodynamic performance-prediction program developed by Boeing Helicopters (ref. 2). This code has been validated through correlations of wind tunnel test data from several rotor systems, in order, in particular, to identify the source and mechanisms of high-harmonic airloads (ref. 3).

The methodology is based on a lifting-line theory with a nonlinear two-dimensional airfoil data base. The blade element approach has been further supplemented by introducing unsteady

aerodynamics with dynamic stall delay and three-dimensional tip relief effects. Blade dynamic response is obtained by solving modal equations of elastic flap and torsional motion. The solution process can be divided into two categories depending on whether the induced flow field is uniform or nonuniform. We first obtain the uniform inflow using simple momentum theory. Then the program trims a rotor iteratively for desired rotor forces. Each iteration loop begins by finding a convergent solution for blade dynamic responses. The uniform downwash solution provides the bound-circulation distribution, Γ_B, of the rotor blade as a function of spanwise locations and azimuth angles. Based on Γ_B, a wake model is developed and the induced inflow velocities are calculated by using the Biot-Savart law. The remainder of the solution process is similar to that for the uniform inflow.

In the nonuniform inflow analysis, one of the blades is allowed to rotate azimuthally and the inflow induced by all vorticities in the rotor flow field is calculated at each azimuth. The blade is called the computation blade, and the wake trailing from this blade is divided into three sections: near, mid, and far wake. The near wake is attached to the blade and is composed of horseshoe vortices shed from each section of the blade. An iterative loop is built around this wake to establish a compatibility between lift and downwash. The midwake region, lying between the near and far regions, is represented by a classical trailing vortex sheet of finite length: typically, about 1/8 of a spiral. It is by now well known that the far wake plays a crucial role in high harmonic airloads. Thus it is natural that B65 has several far-wake models. For this study, the elastically deflected multitrailer wake model, in which vortices are allowed to roll up according to the modified Betz criteria, is used. The number of filaments and the centroid locations are determined by the bound circulation distribution at each azimuth. Therefore, with a negative tip loading, there will be more than one tip vortex filament. The wake trailing from the other blades is approximated by the far wake only. This wake model has been successfully applied to the full-scale H34 wind tunnel test data (ref. 4) and with another Boeing code, C60 (ref. 5).

TFAR1 and TFAR2 CODES

TFAR1 and TFAR2 are potential codes for calculating the steady and unsteady transonic flow past a helicopter rotor blade in hover or in forward flight (ref. 6). TFAR1 predicts only quasi-steady flow, whereas TFAR2 can calculate both types of flow. The codes are based on the full-potential equations in a blade-attached frame of reference. The flow is assumed to be inviscid and isentropic, so there exists a velocity potential. The potential equation can then be solved to yield the three perturbation components of velocity: ϕ_x, ϕ_y, and ϕ_z. The velocities of the blade-fixed reference frame relative to an inertial frame are given by V_1, V_2, and V_3, and the total velocity components of the fluid particle in the moving frame are therefore expressed as

$$\begin{aligned} q_1 &= \phi_x + V_1 \\ q_2 &= \phi_y + V_2 \\ q_3 &= \phi_z + V_3 \end{aligned} \tag{1}$$

TECHNICAL APPROACH

Induced Velocities

The induced velocities from the near, mid, and far wakes are designated as V_{near}, V_{mid}, and V_{far} and are added together to give the total induced velocity at a given computation point on the blade. For the normal and tangential velocities, these are written as

$$\begin{aligned} VN_{tot} &= VN_{near} + VN_{mid} + VN_{far} \\ VT_{tot} &= VT_{near} + VT_{mid} + VT_{far} \end{aligned} \tag{2}$$

where the total normal velocity component, VN_{tot}, acts perpendicular to the rotor disc plane and is positive when directed downward, and the total tangential component, VT_{tot}, acts along the chord length and is positive when directed from leading edge to trailing edge. To compensate for the one-blade near wake effects captured by the potential codes, the induced velocity data from the B65 code must be modified. If, as in the case of the H34 airfoil, a four-bladed rotor is used, then the near wake must be adjusted as follows:

$$\begin{aligned} VN_{tot} &= \frac{3}{4}(VN_{near}) + VN_{mid} + VN_{far} \\ VT_{tot} &= \frac{3}{4}(VT_{near}) + VT_{mid} + VT_{far} \end{aligned} \tag{3}$$

Furthermore, since the B65 velocities are nondimensionalized by the tip speed (ΩR), and the potential code velocities are nondimensionalized by the far field speed of sound (a_∞), then the total induced velocities must be further corrected by the factor ($\Omega R/a_\infty$). The total normal and tangential velocities can then be added to equations (1) in the following manner:

$$\begin{aligned} q_1 &= \phi_x + V_1 \\ q_2 &= \phi_y + V_2 + \left(\frac{\Omega R}{a_\infty}\right) VN_{tot} \\ q_3 &= \phi_z + V_3 + \left(\frac{\Omega R}{a_\infty}\right) VT_{tot} \end{aligned} \tag{4}$$

Inflow Angle

In order to match the theoretical computations with actual flight test results, the correct inflow angle for each azimuth and span station must be extracted from the B65 code and used as input to the potential codes. The total angle of attack is the sum of the geometric and inflow components (ref. 7) and is calculated in B65 as follows:

$$\alpha_{B65} = \Theta_{geometric} + \Phi_{inflow} \tag{5}$$

Since the total normal and tangential induced velocities are added directly to the local flow velocity at the surface of the blade in the potential codes, the effect of these velocities on the angle of attack must be subtracted out as follows:

$$\alpha_{pitch} = \alpha_{B65} - \Phi_{wake} \tag{6}$$

Additionally, since this pitch angle varies along the blade span as well as along the azimuthal position, it must be updated along with the downwash data at each azimuthal calculation when the TFAR2 code is run.

H34 ROTOR

The wake coupling analysis was performed on an H34 four-bladed rotor which consists of a modified NACA0012 airfoil section. Table 1 shows the physical characteristics of the blade which were used as B65 and potential-code input parameters to define the blade geometry.

Table 1. H34 Physical characteristics.

Blade radius	28 ft
Flapping hinge offset	0.0357
Blade cutout	0.16
Blade total twist	$-8°$
Blade type	all metal, constant chord
Airfoil section	modified NACA0012
Blade chord	1.367 ft
Rotor solidity	0.0622
Blade weight	175 lb
Mass moment of inertia	1176 slug-ft^2

The flight test data were obtained from an extensive flight test program using a single-rotor helicopter (ref. 8). The program was conducted at Langley Research Center to obtain helicopter rotor blade airloads, bending moments and blade motion. All data were for trim level flights out of ground effect. The rotor was fully articulated with four H34 blades. Two test flights were selected

to compare the wake coupling analysis results with the flight data. One was for a relatively benign test condition with a forward flight velocity of 92 knots, and the other was for a high-speed flight with a forward velocity of 122 knots. Tables 2 and 3 show the complete test conditions at which the helicopter was operating for these two flights.

Table 2. H34 Flight test conditions at 92 knots.

Flight number	12
Flight velocity	92 knots
Advance ratio	0.25
Rotor tip speed	623 ft/sec
Rotational speed	212 rpm
Shaft inclination	
longitudinal	$-5.1°$
lateral	$-0.9°$
Air density	0.00211 slugs/ft^3
Temperature	68 °F

Table 3. H34 Flight test conditions at 122 knots.

Flight number	20
Flight velocity	122 knots
Advance ratio	0.28
Rotor tip speed	718.38 ft/sec
Rotational speed	245 rpm
Shaft inclination	
longitudinal	$-7.7°$
lateral	$-1.7°$
Air density	0.00212 slugs/ft^3
Temperature	68 °F

The flight test results consisted of pressure data at different chord length (X/C) locations for several span stations (r/R). At r/R = 0.85, pressure orifice locations on the H34 rotor blade were at X/C of 0.017, 0.040, 0.090, 0.130, 0.168, 0.233, 0.335, 0.500, 0.625, 0.769, and 0.915.

BLACK HAWK (UH-60) ROTOR

The wake coupling analysis was also performed on the UH-60 advanced airfoil known as the Black Hawk rotor which consists of the SC1095 and SC1094-R8 airfoil sections. The Black Hawk physical characteristics and airfoil tables were included in the B65 program, and the appropriate

geometric parameters were included in the TFAR2 input data. Since the Black Hawk flight test program is currently under way at Ames Research Center, there is no C_p test data available yet. Therefore only the numerical prediction results are presented. Table 4 shows some of the more important UH-60 physical characteristics. (This information was obtained from the Black Hawk (UH-60) Instrumented Blades Final Design Review Report, by E. I. Seto, 1987.)

Table 4. UH-60 Physical characteristics.

Blade radius	26.833 ft
Flapping hinge offset	0.04660
Blade cutout	0.13043
Blade total twist	$-18°$
Airfoil section	SC1095, SC1094-R8
Blade chord	1.725 ft
Rotor solidity	0.08185
Mass moment of inertia	1229.5 slug-ft^2

The following table shows the simulated flight conditions that were used as input parameters to the wake and potential codes.

Table 5. UH-60 Simulated flight conditions.

Flight velocity	145 knots
Advance ratio	0.34
Rotor tip speed	725 ft/sec
Rotational speed	244.9 rpm
Shaft inclination	
longitudinal	$-2.0°$
lateral	$0.0°$
Air density	0.001921 slugs/ft^3
Temperature	95 °F

RESULTS

Surface-pressure data were obtained for the H34 rotor from the potential codes (TFAR1, TFAR2) with the wake information provided by the B65 code. These data are compared with flight test data from reference 8 which are given as pressure coefficient difference between the lower and upper surfaces of the blade. The results for forward flight velocity of 92 knots are plotted in figure 1 for one complete rotor revolution in azimuthal increments of 30° starting from 0°. The

blade span station at which data were obtained was r/R = 0.85. To show the difference the wake coupling makes to the potential codes, the TFAR2 code was also run without a downwash contribution. These results are plotted in figure 2 for the same azimuthal positions as in the previous case. To further verify the coupling, and to see if there would be any appreciable difference at a more critical flight speed, surface pressure data were also obtained at a forward flight speed of 122 knots. Results for this case are plotted in figure 3.

Additionally, numerical predictions for the UH-60 rotor are presented in figure 4. The results are presented as ΔC_p for Ψ = 0°, 30°, 60°, 90° in figure 4(a) and for Ψ = 120°, 150°, 180°, 210° in figure 4(b).

DISCUSSION

Both TFAR1 and TFAR2 potential codes show good agreement with flight test data, as indicated in figure 1, the TFAR2 results being in closer agreement than those of TFAR1, as anticipated. These res lts are for a forward flight speed of 92 knots with an advance ratio of 0.25. The results of the coupling, however, show a consistent discrepancy of about 6% near the leading edge for most azimuthal angles. It is not clear where this error comes from, but it could theoretically arise from a component of the inflow angle being inadvertently omitted in the calculations. This angle, α_{pitch}, which is used as an input to the potential codes, is defined in equations (5) and (6) and is composed of several terms within its geometric and inflow components. These include such terms as twist angle, collective pitch angle, cyclic pitch angle, and elastic deflection angle, all of which contribute to the total pitch angle. It is reasoned that one of these may have been input incorrectly or not initialized in the computations. Different combinations and options have been tested, but the exact source of the error has not been discovered and the results are presented as they are. The flight test data reduction and accuracy can be found in reference 8, pages 4–6. It should be mentioned that the accuracy of the pressure measurements was estimated to range from 0 to +5%, and the shaft angle measurements were believed to be accurate within ± 0.5°.

In general, excellent agreement is found by TFAR2 for most of the azimuthal range tested. In the region of $90° \leq \Psi \leq 120°$ (figs. 1(d) and 1(e)), the TFAR2 results, while still good, show a deviation from the flight test data. It is reasoned that the error of about 5% may be a result of the high velocities encountered by the advancing blade in this region. These high velocities might affect the theoretical predictions as well as the pressure-sensing devices during flight. TFAR1 results also show this discrepancy, with the problem region expanded to include the region from $30° \leq \Psi \leq 60°$. As can be seen in figures 1(b) and 1(c), the error for the TFAR1 results is between 3% and 5% for this region, and reaches about 10% for $90° \leq \Psi \leq 120°$. Excellent results were obtained with TFAR1, almost as good as those with TFAR2, for the remaining azimuthal locations, namely the region of $150° \leq \Psi \leq 360°$ (figs. 1(f)–1(l)).

Figure 2 shows results of the TFAR2 code with no wake coupling. When TFAR2 was run with no downwash contribution from the wake analysis code, the results overpredicted flight test data on the advancing-blade side from $0° \leq \Psi \leq 180°$ (figs. 2(a)–2(g)) with about 10% to 15% error in the region $60° \leq \Psi \leq 150°$. On the retreating-blade side, TFAR2 underpredicts flight test data from $210° \leq \Psi \leq 330°$ (figs. 2(h)–2(l)) with about 5% error between $240° \leq \Psi \leq 330°$. In

general, these results indicate that wake coupling to the potential codes does indeed increase the agreement with flight test data.

Figure 3 shows the results for the H34 blade at a higher flight speed of 122 knots and an advance ratio of 0.28 for the TFAR2 coupling. The results for each azimuth angle are very similar to those obtained at the lower flight speed of 92 knots. In the leading-edge region, the results are not as good as those obtained at the lower flight speed, but they are within 2% of the previous data, and the higher velocities encountered by the blade may explain the discrepancies. It should also be noted that the flight test data for the high-speed case show some inconsistencies at between 1% and 3% of the chord length for all azimuthal angles, which may explain discrepancies due to flight test accuracy previously mentioned for figures 1(a)–1(l).

The numerical results of TFAR2 with wake coupling are shown in figure 4 for the Black Hawk (UH-60) airfoil with flight conditions as stated in tables 4 and 5. Figure 4(a) shows the numerical prediction of the ΔC_p distribution for $\Psi = 0°$, 30°, 60°, and 90°. As is indicated on the graph, the distribution reaches a maximum of 4.0, decreases for $\Psi = 30°$ and then becomes positive for $\Psi = 60°$ and 90° with a minimum of about 1.2 for $\Psi = 90°$. Figure 4(b) shows the numerical prediction of ΔC_p distribution for $\Psi = 120°$, 150°, 180°, and 210°. In this case, the distribution begins to increase (i.e., become more negative) after $\Psi = 150°$ until it again reaches a maximum of about 4.0 at $\Psi = 210°$.

CONCLUSIONS

The numerical predictions of a rotor potential code can be improved when downwash effects are included in the calculations, since the codes cannot normally capture the downwash effects on their own. A suitable performance and analysis code that generates its own wake can provide these downwash data. It was found that the full unteady TFAR2 code, which accounts for the blade motion, does a better job at predicting the correct airloads than does the quasi-steady TFAR1 code. Furthermore, the more accurately the pitch angle, which can vary both azimuthally and spanwise, is known, the more accurate the results will be. And finally, although the wake coupling to the potential codes give good results at different flight speeds, it was verified that better results are obtained at the lower flight speeds where the advancing blade encounters lower velocities. Overall, the results obtained to date are in good agreement with actual flight test data.

REFERENCES

1. Blaser, D. A.: Pressure Distribution and Angle of Attack Variation on a Helicopter Rotor Blade. American Helicopter Society, vol. 13, 1968, pp. 88-92.

2. Rotor Airloads and Performance Analysis with Non-Uniform Induced Inflow. Boeing Report No. D8-0312, 1968.

3. Dadone, L.: Rotor Wake and BVI Modeling. Helicopter Noise-Reduction Program, NASA CP-2461, 1986.

4. Rabott, J. P.; Lizak, A. A.; and Paglino, V. M.: A Presentation of Measured and Calculated Full Scale Blade Aerodynamics & Structural Loads. USAAVLABS TR66-31, 1966.

5. Oh, B. K.; and Tarzanin, F.: Progress in the Integrated Rotor Noise Prediction System and / irload Correlation. Helicopter Noise-Reduction Program, NASA CP-2461, 1986.

6. Chang, I-C.: Transonic Flow Analysis for Rotors. NASA TP-2375, 1984.

7. Johnson, W.: Helicopter Theory. Princeton University Press, 1980.

8. Scheiman, J.: A Tabulation of Helicopter Rotor-Blade Differential Pressures, Stresses, and Motions as Measured in Flight. NASA TM X-952, 1964.

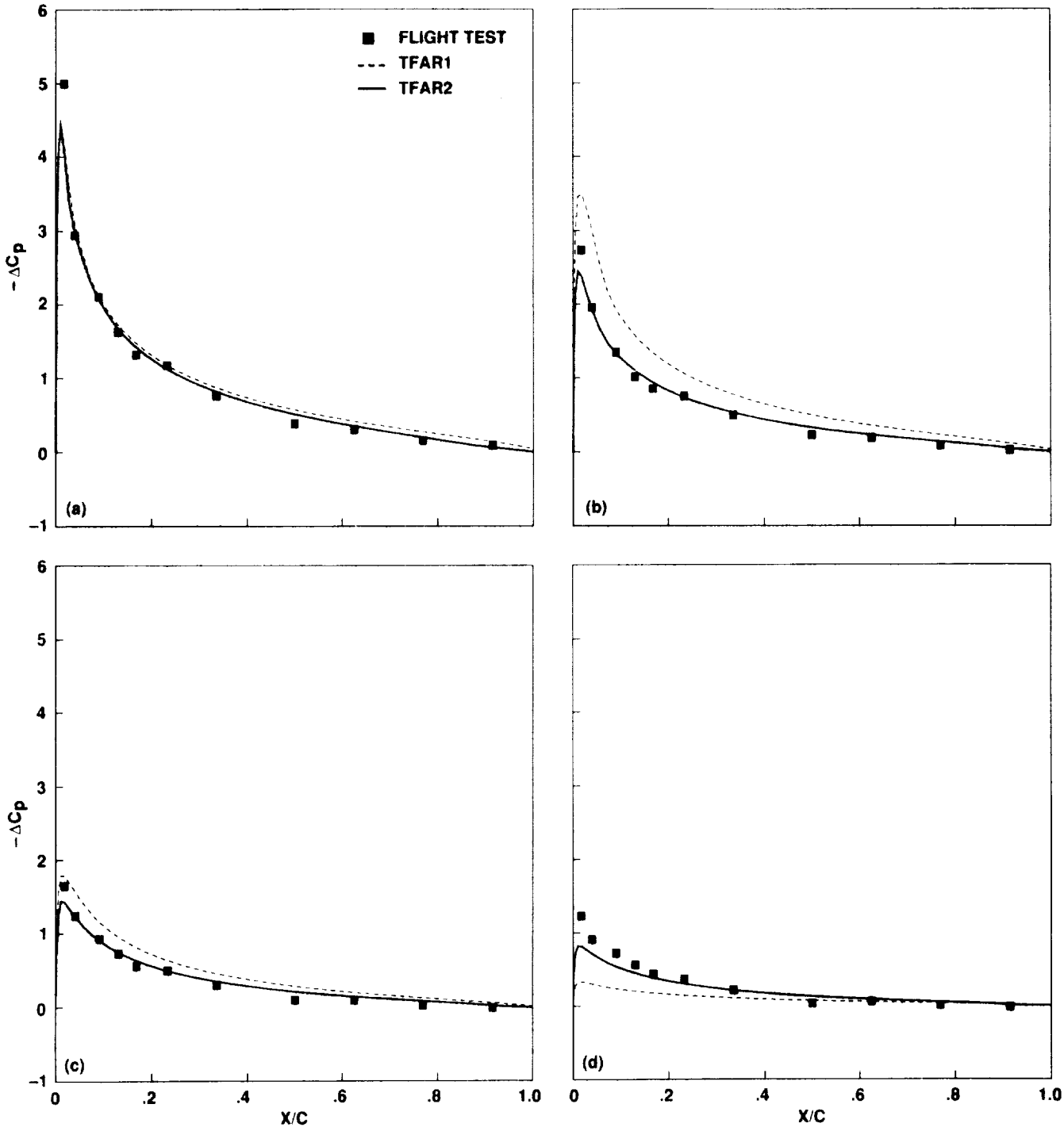

Figure 1. H34 rotor chordwise loading distribution with wake coupling for r/R = 0.85, μ = 0.25, Ωr = 623.0 fps, V = 92 knots. (a) Ψ = 0.0, (b) Ψ = 30.0, (c) Ψ = 60.0, (d) Ψ = 90.0.

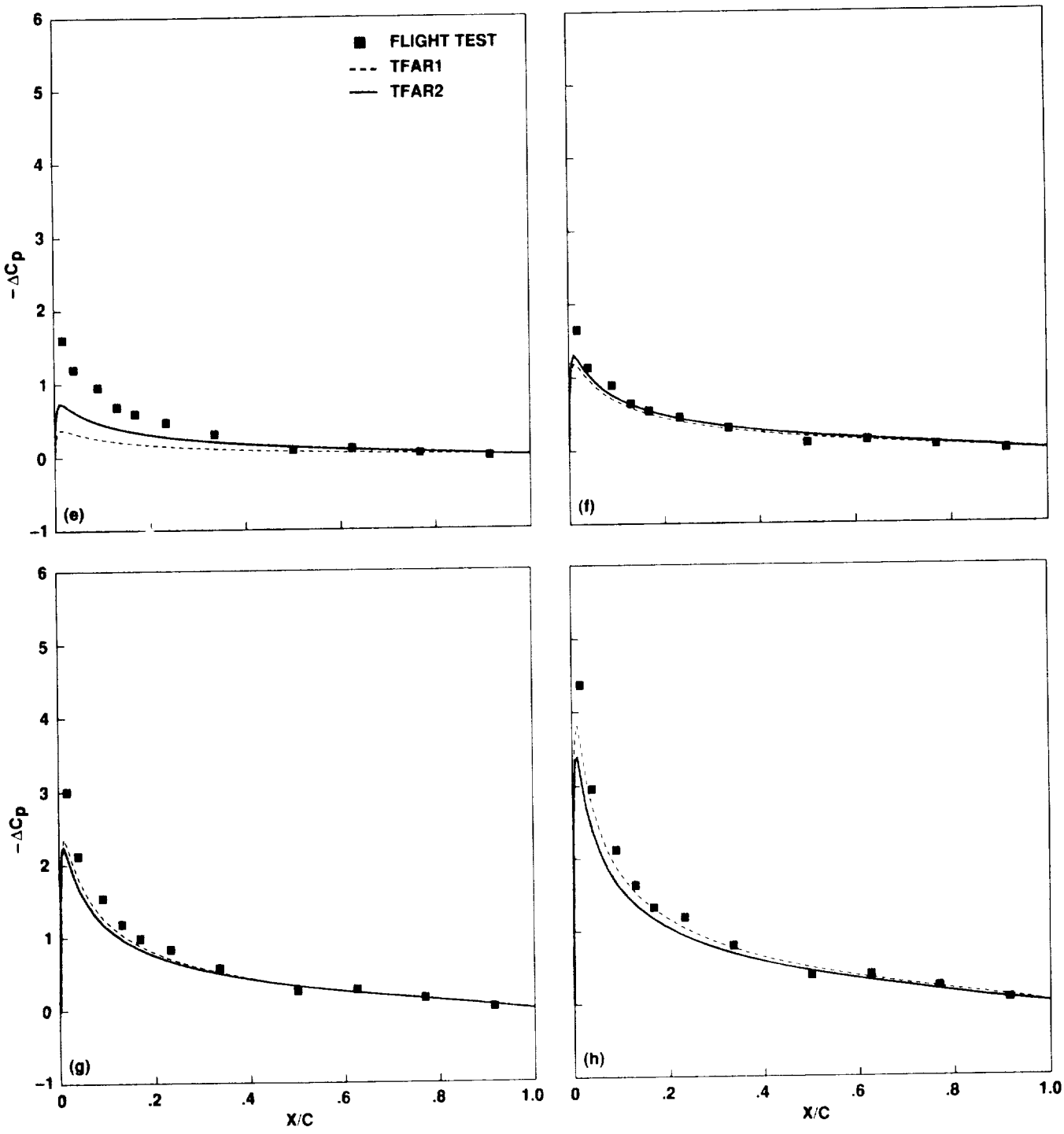

Figure 1. Continued. (e) Ψ = 120.0, (f) Ψ = 150.0, (g) Ψ = 180.0, (h) Ψ = 210.0.

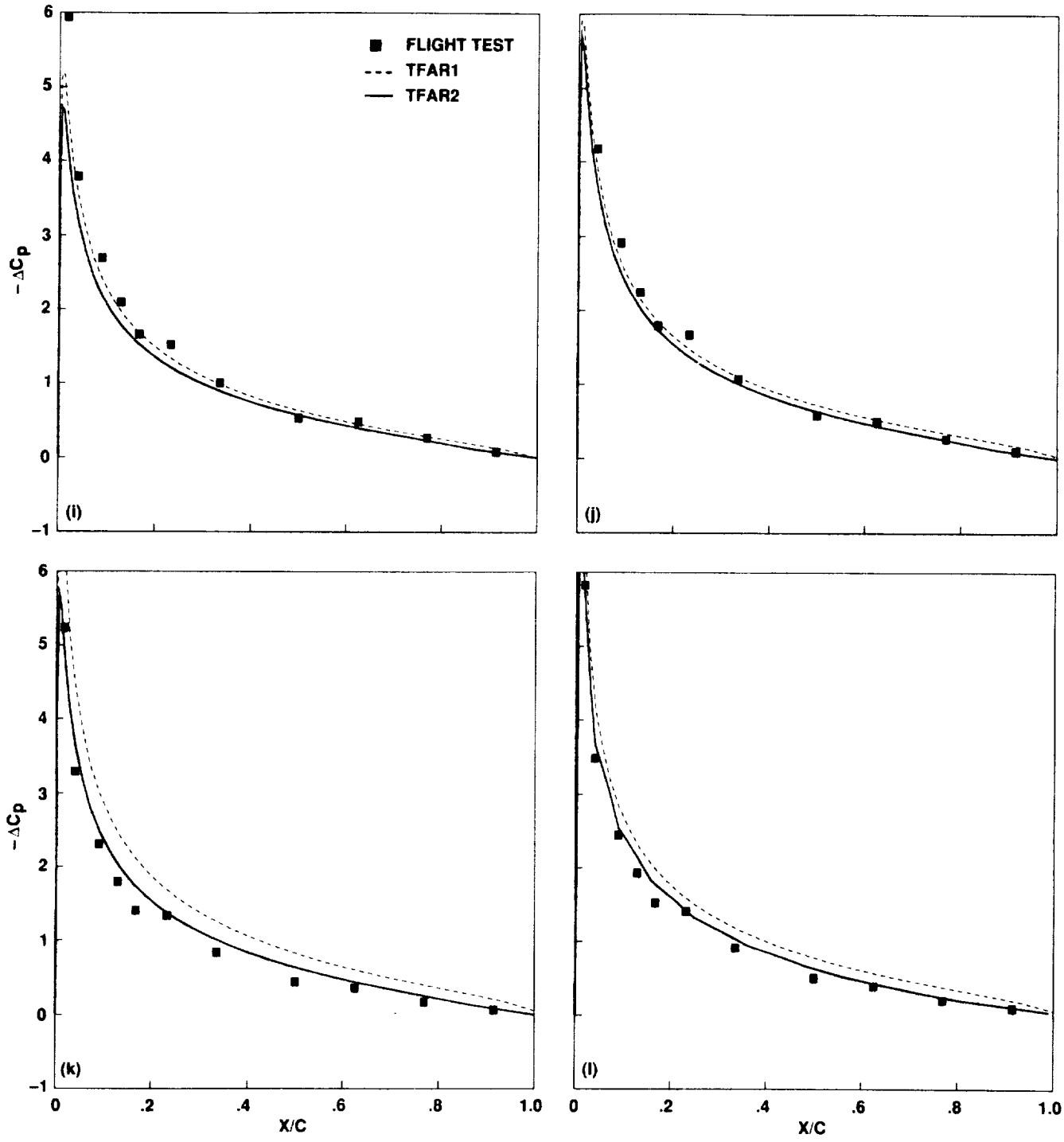

Figure 1. Concluded. (i) Ψ = 240.0, (j) Ψ = 270.0, (k) Ψ = 300.0, (l) Ψ = 330.0.

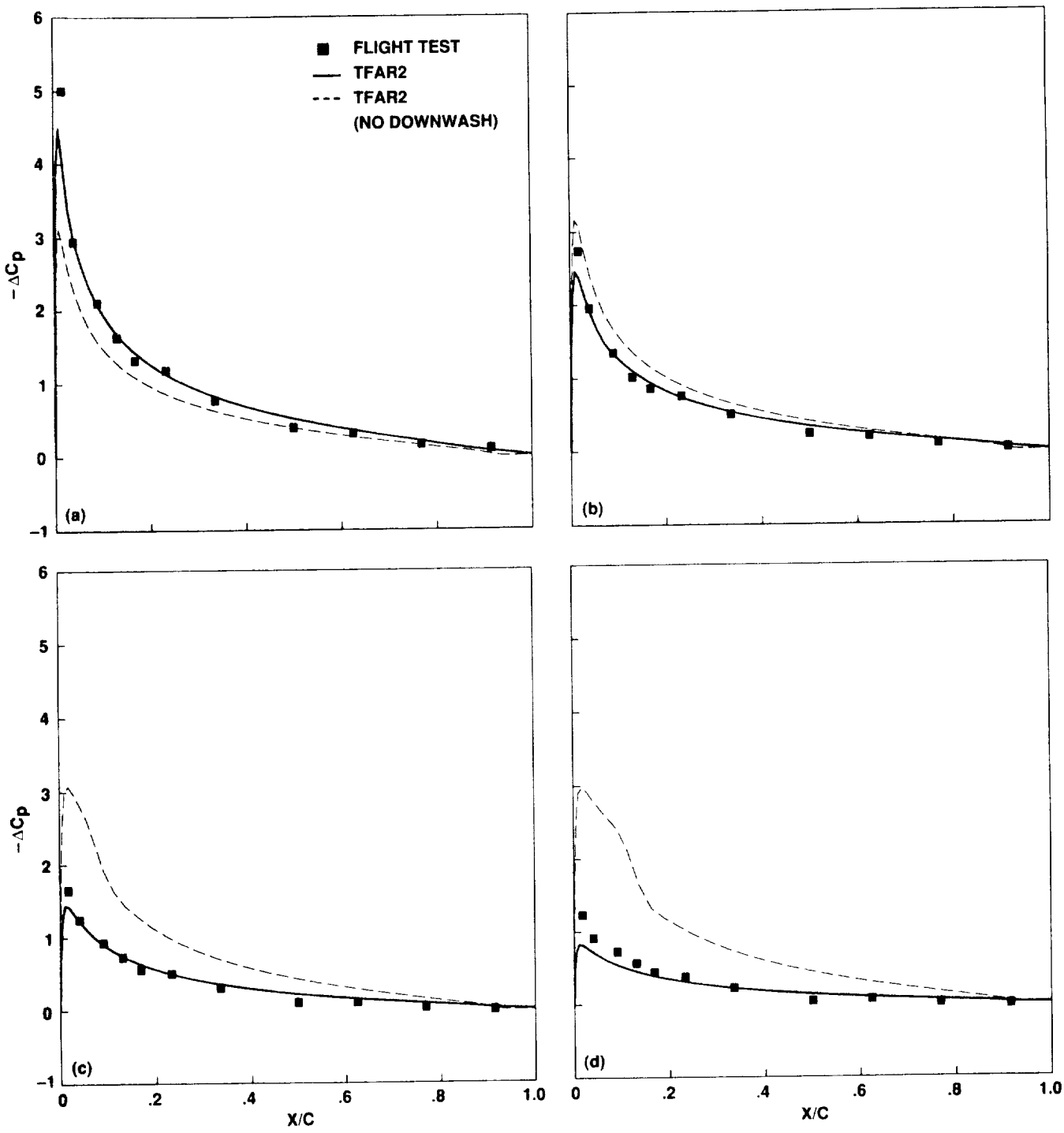

Figure 2. H34 rotor chordwise loading distribution without wake coupling for r/R = 0.85, μ = 0.25, Ωr = 623.0 fps, V = 92 knots. (a) Ψ = 0.0, (b) Ψ = 30.0, (c) Ψ = 60.0, (d) Ψ = 90.0.

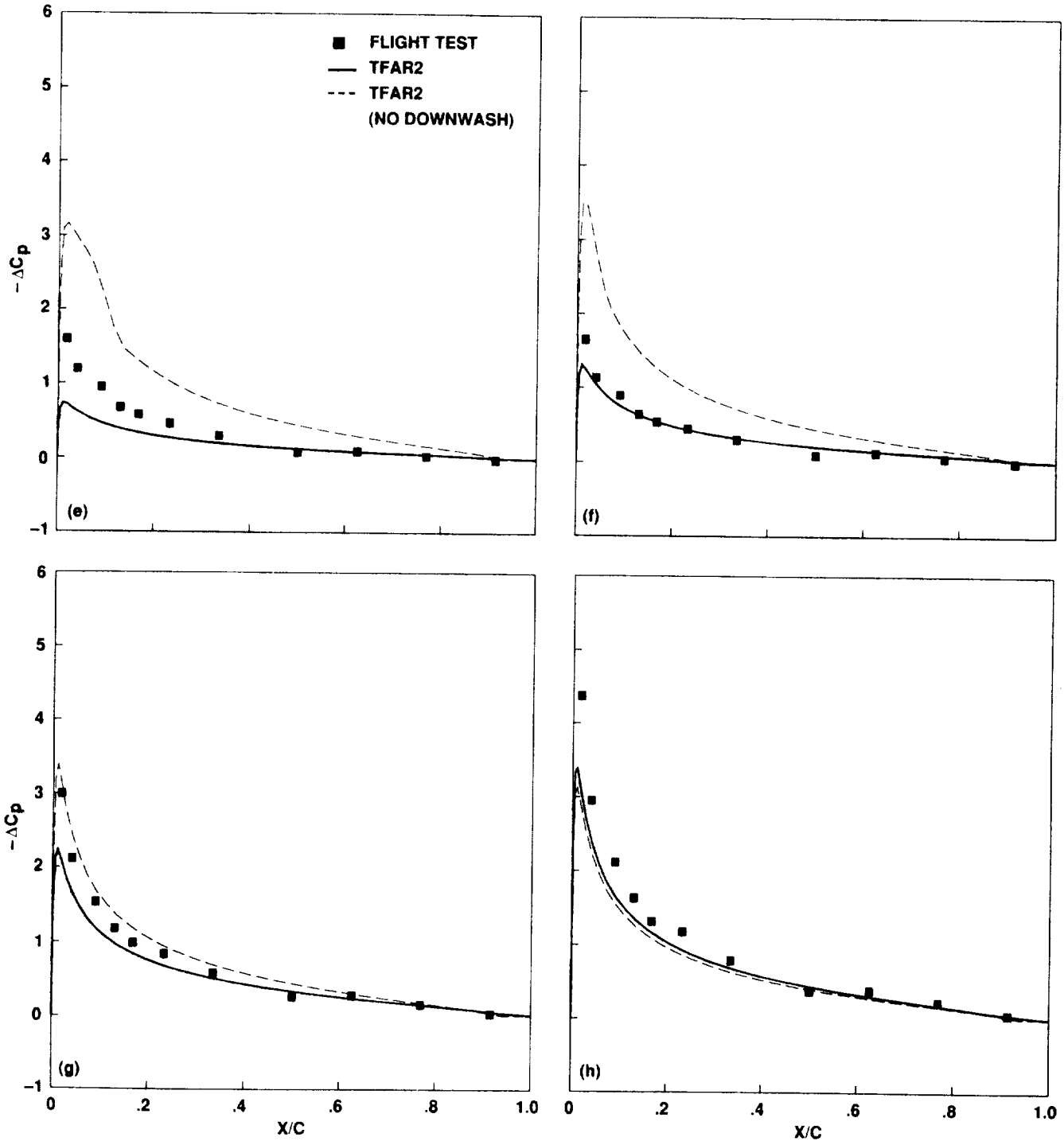

Figure 2. Continued. (e) Ψ = 120.0, (f) Ψ = 150.0, (g) Ψ = 180.0, (h) Ψ = 210.0.

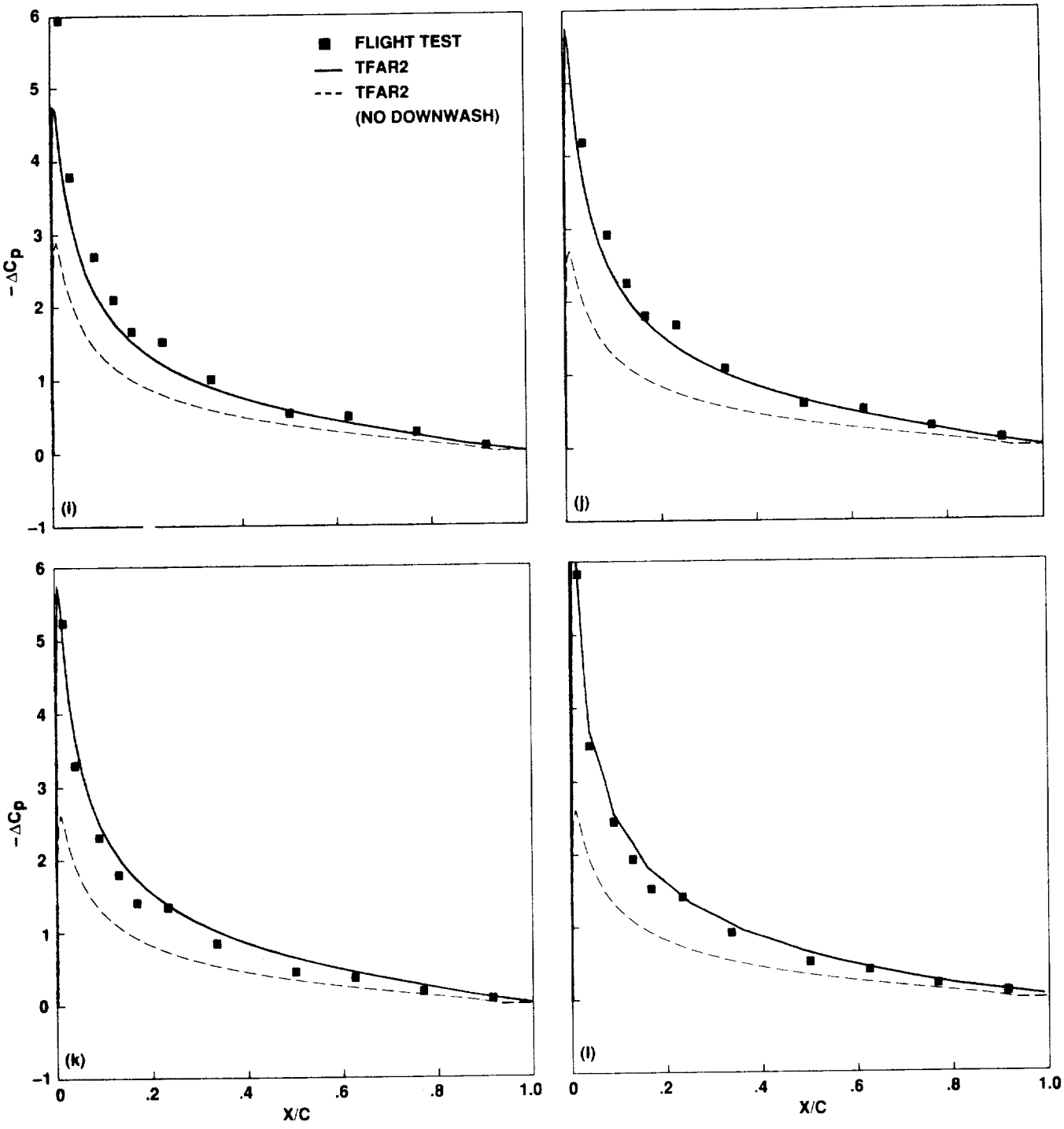

Figure 2. Concluded. (i) Ψ = 240.0, (j) Ψ = 270.0, (k) Ψ = 300.0, (l) Ψ = 330.0.

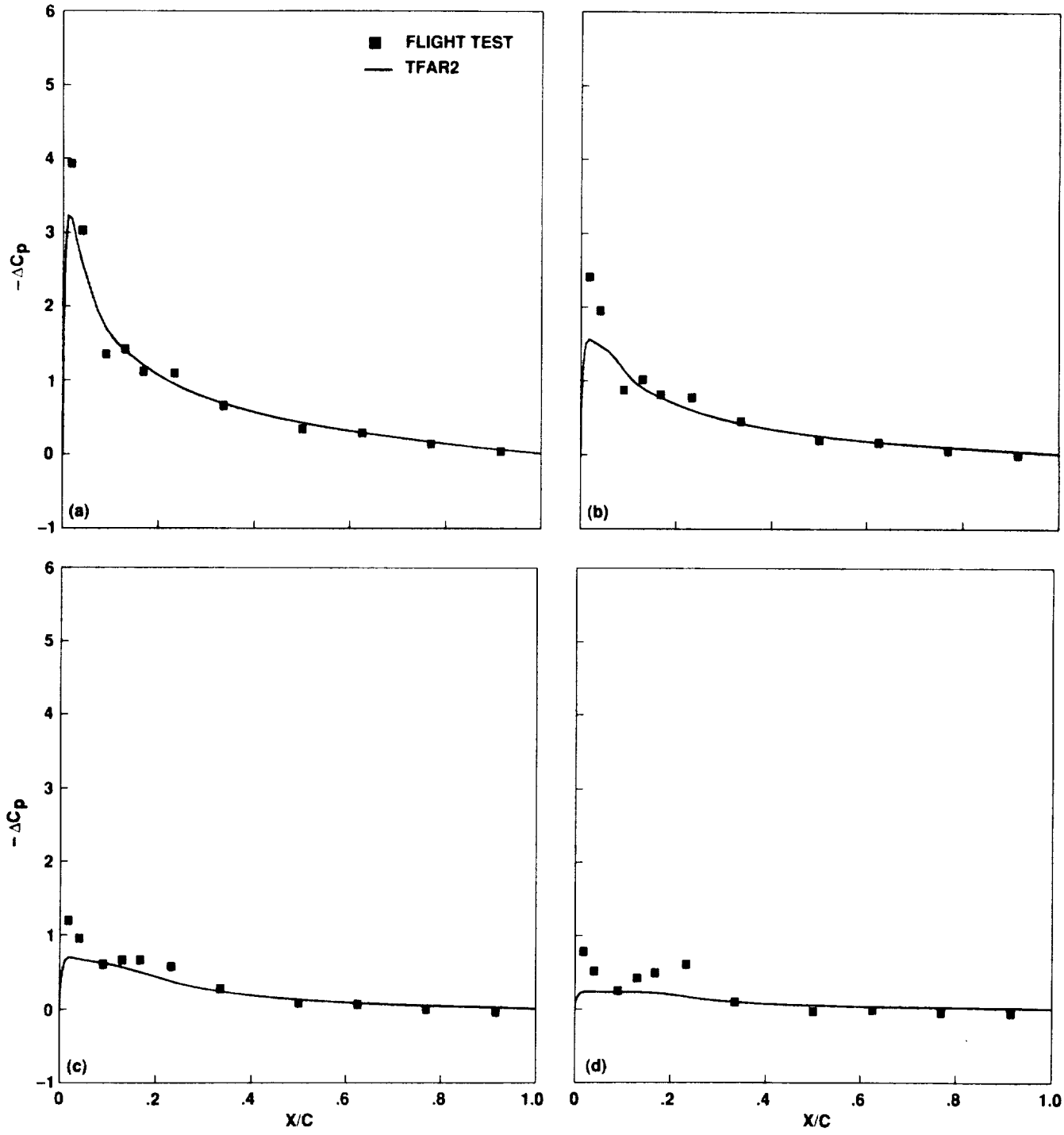

Figure 3. H34 rotor chordwise loading distribution with wake coupling for r/R = 0.85, μ = 0.28, Ωr = 718.38 fps, V = 122 knots. (a) Ψ = 0.0, (b) Ψ = 30.0, (c) Ψ = 60.0, (d) Ψ = 90.0.

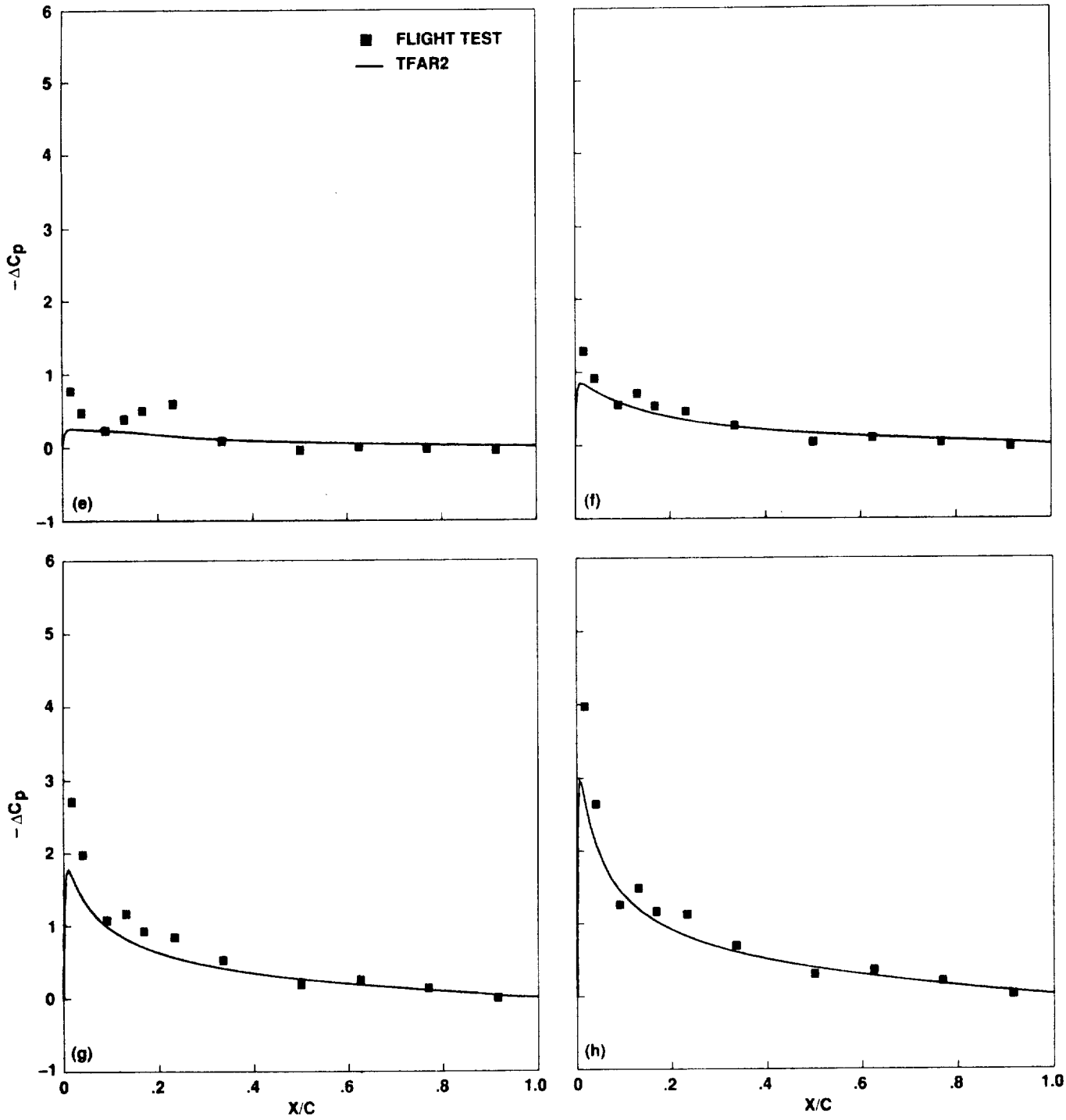

Figure 3. Continued. (e) Ψ = 120.0, (f) Ψ = 150.0, (g) Ψ = 180.0, (h) Ψ = 210.0.

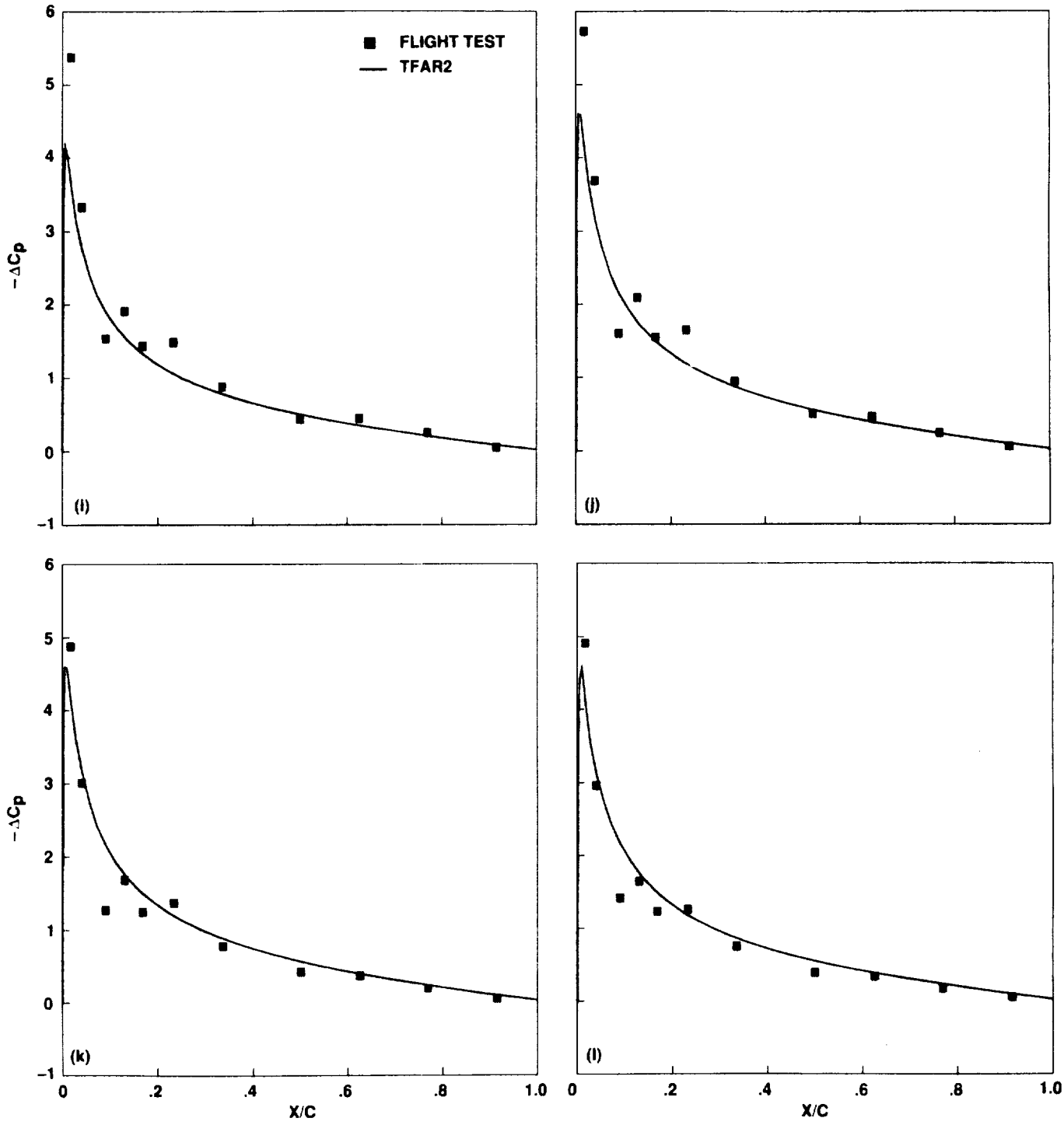

Figure 3. Concluded. (i) Ψ = 240.0, (j) Ψ = 270.0, (k) Ψ = 300.0, (l) Ψ = 330.0.

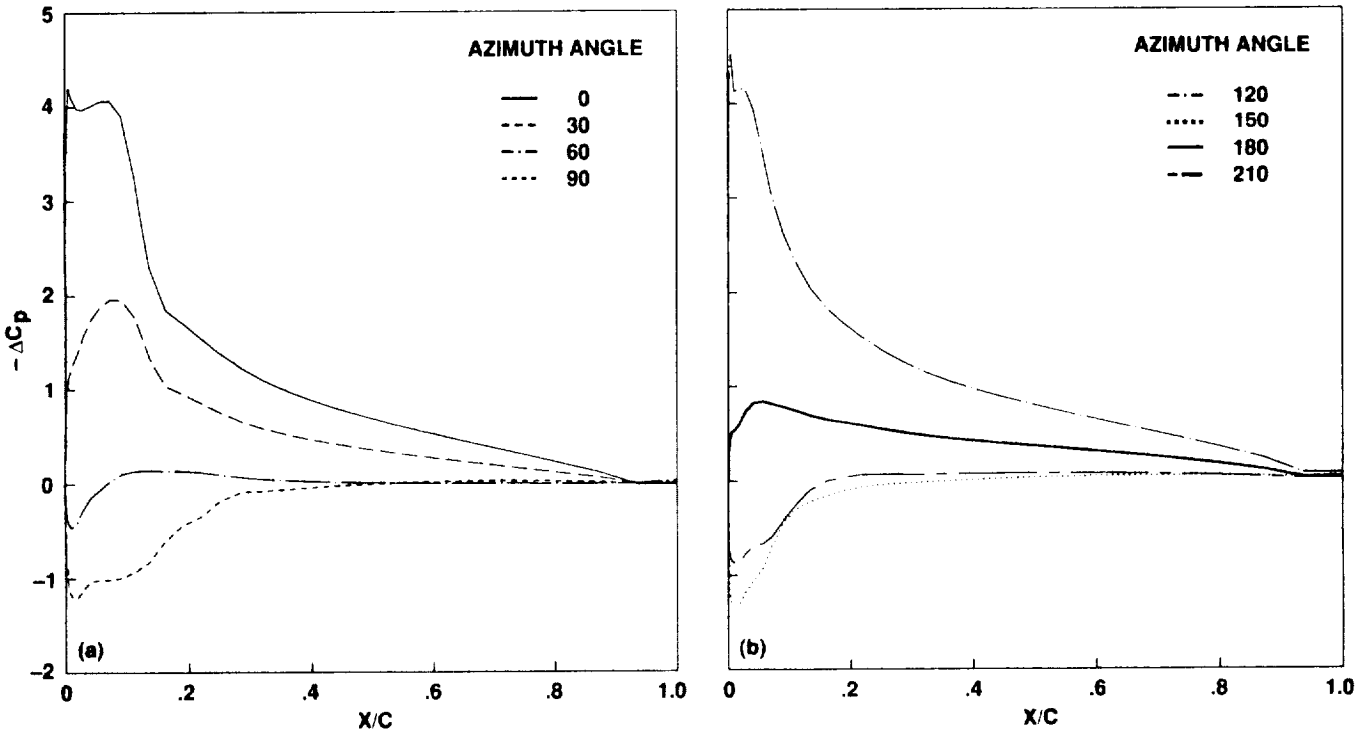

Figure 4. Black Hawk (UH-60) rotor chordwise loading distribution with wake coupling for $\alpha = -2.0$, r/R = 0.85, $\mu = 0.34$, $\Omega r = 725.0$ fps, V = 145 knots.

NASA
National Aeronautics and Space Administration

Report Documentation Page

1. Report No.	2. Government Accession No.	3. Recipient's Catalog No.
NASA TM-102805		

4. Title and Subtitle	5. Report Date
Wake Coupling to Full Potential Rotor Analysis Code	August 1990
	6. Performing Organization Code

7. Author(s)	8. Performing Organization Report No.
Francisco J. Torres, I-Chung Chang, and Byung K. Oh*	A-90117
	10. Work Unit No. 505-60

9. Performing Organization Name and Address	11. Contract or Grant No.
Ames Research Center Moffett Field, CA 94035-1000	
	13. Type of Report and Period Covered Technical Memorandum
12. Sponsoring Agency Name and Address	14. Sponsoring Agency Code
National Aeronautics and Space Administration Washington, DC 20546-0001	

15. Supplementary Notes

Point of Contact: Francisco J. Torres, Ames Research Center, MS 258-2
Moffett Field, CA 94035-1000
(415) 604-4619 or FTS 464-4619

*Boeing Computer Services - Helicopters Support, Philadelphia, Pennsylvania

16. Abstract

The wake information from a helicopter forward flight code is coupled with two transonic potential rotor codes. The induced velocities for the near-, mid-, and far-wake geometries are extracted from a nonlinear rigid wake of a standard performance and analysis code. These, together with the corresponding inflow angles, computation points, and azimuth angles, are then incorporated into the transonic potential codes. The coupled codes can then provide an improved prediction of rotor-blade loading at transonic speeds.

17. Key Words (Suggested by Author(s))	18. Distribution Statement
Transonic flow Helicopter rotor flow Nonlinear wake	Unclassified-Unlimited Subject Category - 02

19. Security Classif. (of this report)	20. Security Classif. (of this page)	21. No. of Pages	22. Price
Unclassified	Unclassified	22	A02

NASA FORM 1626 OCT 86

For sale by the National Technical Information Service, Springfield, Virginia 22161